Chemistry of Metals and Alloys

Chem. Met. Alloys 8 (2015) 75-82
Ivan Franko National University of Lviv
www.chemetal-journal.org

Interaction of the components in the V–{Fe,Ni}–Sn ternary systems

L. ROMAKA[1]*, M. KONYK[1], Yu. STADNYK[1], A. HORYN[1], V.V. ROMAKA[2], R. SERKIZ[1], V. KRAYOVSKYY[2]

[1] *Department of Inorganic Chemistry, Ivan Franko National University of Lviv, Kyryla i Mefodiya St. 6, 79005 Lviv, Ukraine*
[2] *Department of Materials Engineering, Lviv Polytechnic National University, Ustyyanovycha St. 5, 79013 Lviv, Ukraine*
* *Corresponding author. E-mail: romakal@lnu.edu.ua*

Received September 10, 2015; accepted December 30, 2015; available on-line September 19, 2016

The phase equilibria of the V–Fe–Sn and V–Ni–Sn ternary systems at 873 K and 773 K, respectively, were studied in the whole concentration range, using X-ray diffraction and metallographic analysis. The V–Fe–Sn ternary system at 873 K is characterized by the formation of two ternary intermetallic compounds, VFe_2Sn ($MnCu_2Al$-type, space group *Fm*-3*m*, *a* = 0.59641(3) nm) and $(V,Fe)Sn_2$ (Mg_2Ni-type, space group *P*6$_2$22, *a* = 0.5441(1)-0.5437(1), *c* = 1.3852(2)-1.3769(5) nm). In the V–Ni–Sn system at 773 K only one ternary compound, VNi_2Sn ($MnCu_2Al$-type, *a* = 0.6031(1) nm), was observed. Electrical resistivity and thermopower were measured for the $(V,Fe)Sn_2$ compound in the temperature range 80-380 K. The compound shows metallic type of conductivity in the investigated temperature range.

Stannides / Phase diagram / EPMA / Electrical properties / X-ray powder diffraction

1. Introduction

Ternary systems with vanadium, *d*-metals and *p*-elements are interesting objects for investigation. The equiatomic compounds VCoSb and VFeSb crystallize with the cubic MgAgAs type (so-called half-Heusler phases) and constitute the basis of many semiconducting materials for thermoelectric applications [1-4]. It was shown in [4] that the VFeSb compound, and related multi-component substitutional alloys based on this ternary phase, may be considered as promising moderate-temperature thermoelectric materials. For the full-Heusler phases VM_2X ($MnCu_2Al$-type), found with *M* = Fe, Co, Ni; *X* = Ga, Sn, the magnetic and the magneto-optical properties have already been investigated [5-7]. The VNi_2Sn compound is characterized by Pauli paramagnetism and metallic type of conductivity [8]. In [9] the $(V,Fe)_{3.4}Sn_{0.6}$ ternary phase with $MnCu_2Al$-type structure and a large homogeneity range was reported at low Sn content (15 at.%). The V–Ni–Sn phase diagram was studied at 1070 K [10] and a wide composition range was found for the VNi_2Sn intermetallic (from 24.6 at.% to 49.6 at.% V, from 50.6 at.% to 31.2 at.% Ni, and from 24.8 at.% to 19.2 at.% Sn).

In this context it is important to investigate the V–*M*–Sn phase diagrams, and to study for each phase its stability (composition and temperature range), the influence of the size factor and preparation methods.

In this paper we present the results of an X-ray diffraction and EPMA investigation of the phase equilibria in the V–Fe–Sn ternary system at 873 K, and in the V–Ni–Sn system at 773 K. Taking into account the above literature data, which indicates the formation of the VFe_2Sn compound at the stoichiometric composition at 873 K and 1073 K [5,7], the phase equilibria in the V–Fe–Sn system were studied at 873 K.

2. Experimental

The samples were prepared by direct arc melting of the constituent elements (vanadium, purity 99.96 wt.%; iron, 99.99 wt.%; nickel, 99.99 wt.%; tin, 99.999 wt.%) under high-purity, Ti-gettered argon atmosphere on a water-cooled copper hearth. The alloys were annealed at 773 K (V–Ni–Sn alloys), or at 873 K (V–Fe–Sn alloys), in evacuated quartz tubes for 720 h, and subsequently quenched in ice water.

X-ray phase analysis of the samples was carried out using powder patterns obtained on a DRON-4.0 diffractometer (Fe *Kα* radiation). The observed diffraction intensities were compared with reference powder patterns of known binary and ternary phases. The lattice parameters were refined by least-squares fits of indexed 2*θ*-values, using the WinCSD program package [11].

The chemical compositions of the samples were examined by Scanning Electron Microscopy (SEM), using a REMMA-102-02 scanning electron microscope. Quantitative electron probe microanalysis (EPMA) of the phases was carried out by using an energy-dispersive X-ray analyzer with the pure elements as standards (the acceleration voltage was 20 kV; *K*- and *L*-lines were used).

The electrical resistivity was measured in the temperature range 80-380 K, employing the two-probe method on millimeter-scale, well-shaped pieces, cut by spark erosion from polycrystalline samples. Thermoelectric power measurements were carried out using a standard differential method with pure copper as reference material, in the temperature range 80-380 K.

3. Results and discussion

3.1. Isothermal section of the phase diagram of the V–Fe–Sn system at 873 K

The phase equilibria in the V–Fe–Sn system were investigated in the whole concentration range at 873 K, using X-ray diffraction and metallographic analysis of 6 binary and 28 ternary alloys. The isothermal section of the V–Fe–Sn phase diagram at this temperature is presented in Fig. 1. The phase compositions of selected samples are listed in Table 1; microphotographs of some alloys are shown in Fig. 2.

In the course of an investigation of the Fe–Sn system at 873 K, we confirmed the existence of the Fe_3Sn_2 (Fe_3Sn_2-type) and FeSn (CoSn-type) binaries [12-14]. In the V–Sn system two binary phases, i.e. VSn_2 (Mg_2Cu-type) and V_3Sn, adopting a modification of the cubic Cr_3Si-type, were observed at 873 K, in agreement with [12,15].

In the V–Fe binary system the VFe phase ($V_{0.5}Fe_{0.5}$, $Cr_{0.49}Fe_{0.51}$-type, ~33-65 at.% V) was successfully synthesized and confirmed at the investigated temperature. Crystallographic characteristics of the binary phases are listed in Table 2. The solubility of the third component in the binary compounds was not significant under our conditions, except for V_3Sn (Cr_3Si-type), for which the solubility of Fe reached 7 at.% (limiting composition according to EPMA: $V_{67.47}Fe_{6.82}Sn_{25.71}$, a = 0.4967(1)-0.4932(4) nm). The sample of composition $V_{65}Fe_5Sn_{30}$ (Fig. 2a) is located in a two-phase region and contains as main phase $V_{3-x}Fe_xSn$, in equilibrium with the VSn_2 binary compound.

The existence of the already known VFe_2Sn ($MnCu_2Al$-type) and $(V,Fe)Sn_2$ (Mg_2Ni-type) [5,21] compounds was confirmed at 873 K. Under the conditions used here, the VFe_2Sn compound was observed at the stoichiometric composition. According to X-ray diffraction and EPMA data, the $(V,Fe)Sn_2$ phase is characterized by a small homogeneity region along the 66.7 at.% Sn isoconcentrate, delimited by the compositions $V_{0.55}Fe_{0.45}Sn_2$ ($V_{18.14}Fe_{15.27}Sn_{66.59}$; Fig. 2c) and $V_{0.51}Fe_{0.49}Sn_2$ ($V_{16.85}Fe_{16.03}Sn_{67.12}$; Fig. 2d). The crystallographic characteristics of the V–Fe–Sn ternary compounds are listed in Table 3.

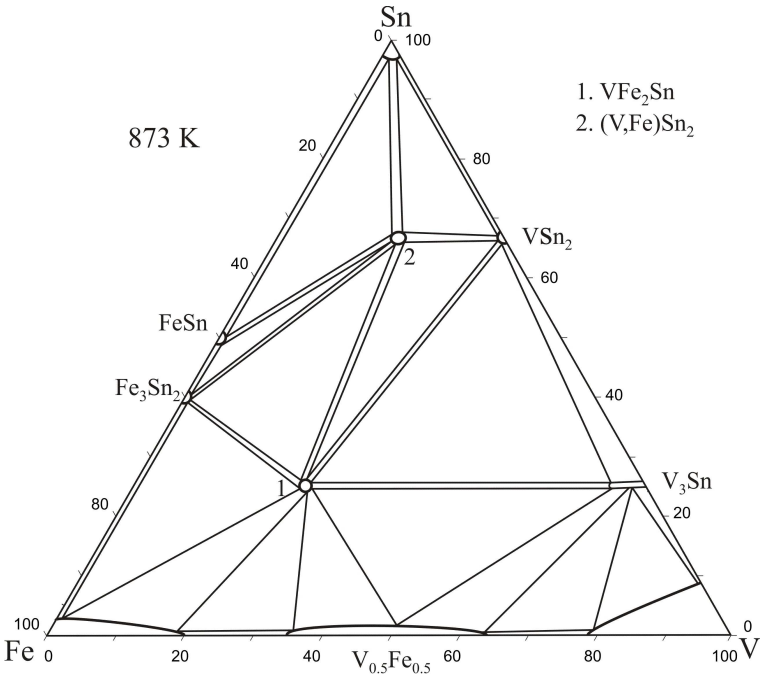

Fig. 1 Isothermal section of the phase diagram of the V–Fe–Sn system at 873 K.

Table 1 Phase compositions of selected V–Fe–Sn alloys annealed at 873 K.

No.	Nominal alloy composition (at.%)			Phases		
	V	Fe	Sn	1st phase	2nd phase	3rd phase
1	20	65	15	VFe_2Sn a = 0.5955(4) nm	(Fe,V) a = 0.2875(3)	
2	30	55	15	VFe_2Sn a = 0.5953(3) nm	(Fe,V) a = 0.2878(4)	VFe ($V_{0.5}Fe_{0.5}$) (traces)
3	60	10	30	V_3Sn a = 0.4935(4) nm	VSn_2 a = 0.9486(3) nm b = 0.5484(3) nm c = 1.8674(5) nm	VFe_2Sn a = 0.5957(4) nm
4	15	55	30	VFe_2Sn a = 0.5957(3) nm	Fe_3Sn_2 a = 0.5351(4) nm c = 1.9849(7) nm	
5	20	40	40	VFe_2Sn a = 0.5959(3) nm	Fe_3Sn_2 a = 0.5350(3) nm c = 1.9847(6) nm	$(V,Fe)Sn_2$ (traces)
6	40	15	45	VSn_2 a = 0.9485(4) nm b = 0.5486(3) nm c = 1.8676(5) nm	VFe_2Sn a = 0.5958(3) nm	V_3Sn a = 0.4935(4) nm
7	3	50	47	FeSn a = 0.5296(3) nm c = 0.4480(3) nm	Fe_3Sn_2 a = 0.5352(4) nm c = 1.9851(6) nm	$(V,Fe)Sn_2$ (traces)
8	25	25	50	$(V,Fe)Sn_2$ a = 0.5438(2) nm c = 1.3766(9) nm	VFe_2Sn a = 0.5957(4) nm	VSn_2 a = 0.9487(4) nm b = 0.5487(4) nm c = 1.8676(5) nm
9	23	15	62	$(V,Fe)Sn_2$ a = 0.5437(2) nm c = 1.3761(7) nm	VSn_2 a = 0.9487(4) nm b = 0.5487(4) nm c = 1.8678(6) nm	VFe_2Sn a = 0.5956(5) nm
10	17	13	70	$(V,Fe)Sn_2$ a = 0.5438(2) nm c = 1.3760(6) nm	Sn a = 0.5933(9) nm c = 0.3281(7) nm	

Table 2 Binary phases relevant to the isothermal sections of the V–Fe–Sn and V–Ni–Sn systems.

Phase	Melting / transformation temperature (°C) [12]	Pearson symbol, structure type	Lattice parameters, nm			Ref.
			a	b	c	
VSn_2	p 756°C	$oF48$, Mg_2Cu	0.9487(4)	0.5486(1)	1.8675(3)	This work
V_3Sn	p ~1600°C	$cP8$, Cr_3Si	0.4967(1)	–	–	This work
VFe	pm 1252°C	$tP30$, CrFe	0.8965	–	0.4633	[16]
Fe_3Sn_2	p 806°C	$hR30$, Fe_3Sn_2	0.5344	–	1.9845	[17]
	ed 607°C		0.5378(1)		1.9736(6)	This work
FeSn	p 770°C	$hP6$, CoSn	0.5295(1)	–	0.4449(8)	This work
VNi_3	pm 1045°C	$tI8$, $TiAl_3$	0.3543	–	0.7221	[18]
VNi_2	pm 922°C	$oI6$, $MoPt_2$	0.2567(3)	0.3535(5)	0.7689(7)	This work
$V_{0.7}Ni_{0.3}$	pm 790°C	$tP30$, $Cr_{0.49}Fe_{0.51}$	0.9038(6)	–	0.4663(5)	This work
V_3Ni	pd 900°C	$cP8$, Cr_3Si	0.4710	–	1.0449	[19]
Ni_3Sn	pm 975°C	$hP8$, Mg_3Cd	0.5305	–	0.4254	[20]
ht-Ni_3Sn_2	m ~1250°C	$hP6$, Ni_2In	0.4087(1)	–	0.5159(2)	This work
Ni_3Sn_4	p 795°C	$mS14$, Ni_3Sn_4	1.2225(6)	0.4064(4) β = 103.9°	0.5188(4)	This work

* p – peritectic reaction; pd – peritectoid reaction; pm – polymorphic transformation; m – congruent melting; ed – eutectoid decomposition.

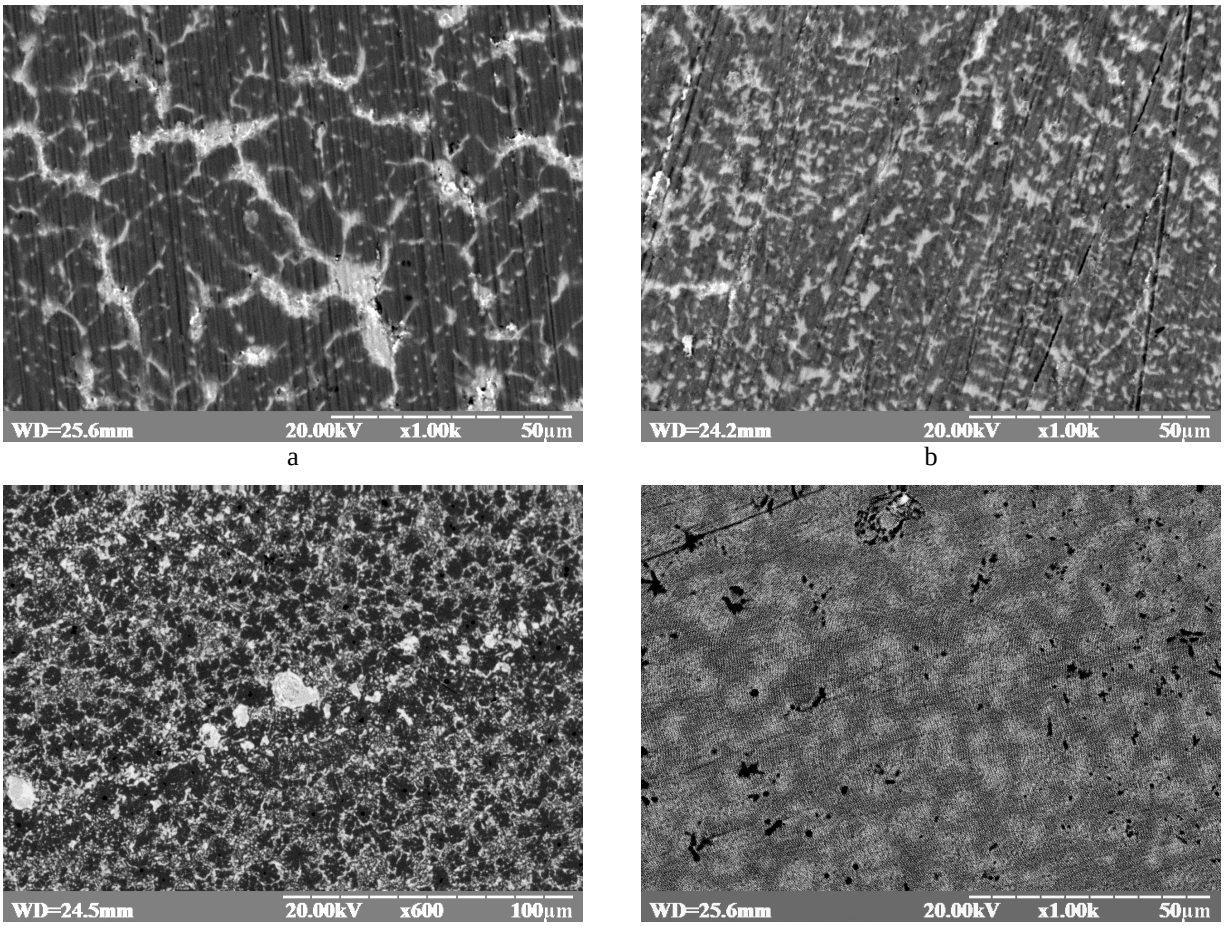

Fig. 2 SEM photographs of alloys from the V–Fe–Sn system: a) $V_{65}Fe_5Sn_{30}$ – $V_{3-x}Fe_xSn$ ($V_{67.47}Fe_{6.82}Sn_{25.71}$, dark), VSn_2 (light); b) $V_{50}Fe_{15}Sn_{35}$ – VSn_2 (light), V_3Sn (grey), VFe_2Sn (dark); c) $V_{25}Fe_{45}Sn_{30}$ – VFe_2Sn (dark), $(V,Fe)Sn_2$ ($V_{18.14}Fe_{15.27}Sn_{66.59}$, light grey), VSn_2 (light); d) $V_{17}Fe_{13}Sn_{70}$ – $(V,Fe)Sn_2$ ($V_{16.65}Fe_{16.12}Sn_{67.21}$, grey), Sn (light).

Table 3 Crystallographic characteristics of the V–Fe–Sn and V–Ni–Sn ternary compounds.

No.[a]	Compound	Space group	Structure type	Lattice parameters, nm		
				a	*b*	*c*
1	VFe_2Sn	*Fm*-3*m*	$MnCu_2Al$	0.59641(3)	-	
2	$V_{0.55}Fe_{0.45}Sn_2$–$V_{0.51}Fe_{0.49}Sn_2$	*P*6$_2$22	Mg_2Ni	0.5441(1)–0.5437(1)	-	1.3852(5)–1.3769(7)
1	VNi_2Sn	*Fm*-3*m*	$MnCu_2Al$	0.6031(1)	-	

[a] The compound numbers correspond to the phase diagrams (Fig. 1, Fig. 3).

3.2. Isothermal section of the phase diagram of the V–Ni–Sn system at 773 K

The phase equilibria of the V–Ni–Sn ternary system were investigated at 773 K, using X-ray diffraction and EPMA data of 34 binary and ternary alloys. The isothermal section of the V–Ni–Sn phase diagram is presented in Fig. 3. The phase compositions of selected samples are listed in Table 4, and microphotographs of some alloys are shown in Fig. 4.

The version of the Ni–Sn phase diagram and crystallographic data of the binary compounds, accepted here, are taken from the handbooks edited by Massalski et al. [12] and Villars and Calvert [13]. At 773 K three phases are known: Ni_3Sn (Mg_3Cd-type), Ni_3Sn_4 (Ni_3Sn_4-type), and Ni_3Sn_2 (Ni_2In-type). To check the existence of the NiSn binary stannide [22], samples of compositions $Ni_{50}Sn_{50}$ and $Ni_{48}Sn_{52}$ were prepared and annealed at 770, 870, and 1070 K. Phase analysis of the samples showed the presence of two phases: Ni_3Sn_4 and Ni_3Sn_2 at all the investigated temperatures. In the V–Sn system the two binary phases VSn_2 (Mg_2Cu-type) and V_3Sn (Cr_3Si-type) were confirmed at 773 K.

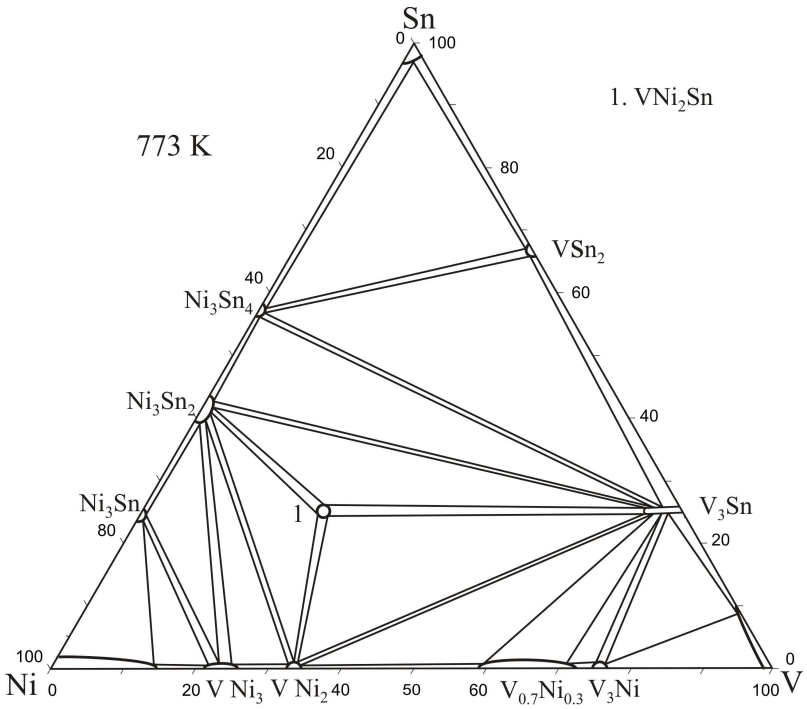

Fig. 3 Isothermal section of the phase diagram of the V–Ni–Sn system at 773 K.

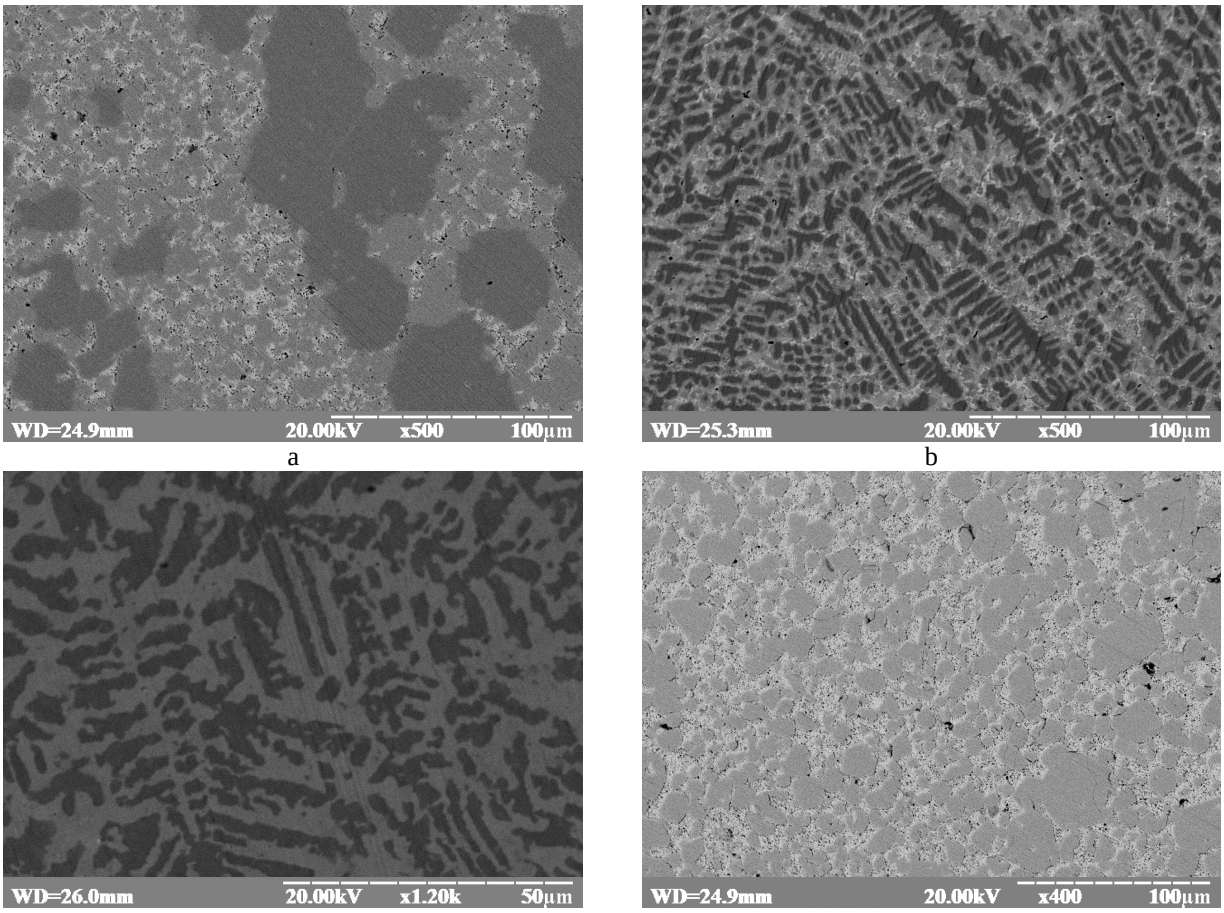

Fig. 4 SEM photographs of alloys from the V–Ni–Sn system: a) $V_{27}Ni_7Sn_{66}$ – VSn_2 (grey), Ni_3Sn_4 (dark), Sn (light); b) $V_{70}Ni_{10}Sn_{20}$ – V_3Sn ($V_{67.24}Ni_{7.58}Sn_{25.18}$, dark), $V_{0.7}Ni_{0.3}$ (grey), VNi_2 (light); c) $V_{50}Ni_{20}Sn_{30}$ – V_3Sn (dark), Ni_3Sn_2 (grey); d) $V_{15}Ni_{45}Sn_{40}$ – Ni_3Sn_2 (grey), V_3Sn (dark), Ni_3Sn_4 (light).

Table 4 Phase compositions of selected V–Ni–Sn alloys annealed at 773 K.

No.	Nominal alloy composition (at.%)			Phases		
	V	Ni	Sn	1st phase	2nd phase	3rd phase
1	25	60	15	Ni_3Sn_2 *a* = 0.4102(1) nm *b* = 0.5182(1) nm	VNi_2Sn *a* = 0.6044(4) nm	VNi_2 *a* = 0.2563(3) nm *b* = 0.7679(4) nm *c* = 0.3533(3) nm
2	40	45	15	VNi_2Sn *a* = 0.6050(2) nm	V_3Sn *a* = 0.4943(3) nm	VNi_2 (traces)
3	20	65	15	Ni_3Sn_2 *a* = 0.4098(4) nm *c* = 0.5180(3) nm	VNi_3 *a* = 0.3519(2) nm *c* = 0.7180(4) nm	VNi_2 *a* = 0.2560(2) nm *b* = 0.7681(5) nm *c* = 0.3531(4) nm
4	20	55	25	VNi_2Sn *a* = 0.6034(3) nm	Ni_3Sn_2 *a* = 0.4102(1) nm *c* = 0.5180(2) nm	VNi_2 *a* = 0.2561(4) nm *b* = 0.7677(5) nm *c* = 0.3534(4) nm
5	55	15	30	V_3Sn *a* = 0.4942(4) nm	Ni_3Sn_2 *a* = 0.4101(1) nm *c* = 0.5182(1) nm	
6	15	50	35	Ni_3Sn_2 *a* = 0.4102(1) nm *c* = 0.5181(1) nm	VNi_2Sn *a* = 0.6033(2) nm	V_3Sn *a* = 0.4941(4) nm
7	20	35	45	Ni_3Sn_2 *a* = 0.4088(2) nm *c* = 0.5177(3) nm	V_3Sn *a* = 0.4953(3) nm	Ni_3Sn_4 (traces)
8	10	40	50	Ni_3Sn_4 *a* = 1.2227(6) nm *b* = 0.4068(4) nm *c* = 0.5191(4) β = 103.8(3)°	Ni_3Sn_2 *a* = 0.4083(4) nm *c* = 0.5163(4) nm	V_3Sn (traces)
9	35	15	50	VSn_2 *a* = 0.9496(3) nm *b* = 0.5481(3) nm *c* = 1.8673(5) nm	Ni_3Sn_4 *a* = 1.2225(6) nm *b* = 0.4064(4) nm *c* = 0.5188(4) β = 103.9(3)°	V_3Sn *a* = 0.4953(4) nm
10	23	10	67	VSn_2 *a* = 0.9497(4) nm *b* = 0.5483(3) nm *c* = 1.8675(6) nm	Ni_3Sn_4 *a* = 1.2224(7) nm *b* = 0.4067(4) nm *c* = 0.5192(4) β = 103.9(3)°	Sn *a* = 0.5933 (9) nm *c* = 0.3281(7) nm

In the V–Ni system four binary phases, i.e. VNi_3 ($TiAl_3$-type), VNi_2 ($MoPt_2$-type), $V_{0.7}Ni_{0.3}$ ($Cr_{0.49}Fe_{0.51}$-type), and V_3Ni (Cr_3Si-type), were observed at 773 K, in agreement with [12,13]. Crystallographic characteristics of the binary phases are listed in Table 2. The formation of a solid solution $V_{3-x}Ni_xSn$ by substitution of Ni for V in the V_3Sn binary up to 7.5 at.% was found under the conditions used here (limiting composition according to EPMA: $V_{67.24}Ni_{7.58}Sn_{25.18}$, *a* = 0.4971(4)-0.4942(4) nm). The sample of composition $V_{50}Ni_{20}Sn_{30}$ contained two phases in equilibrium: V_3Sn and Ni_3Sn_2 (Fig. 4c). The maximum solubility of vanadium in the Ni_3Sn_2 phase was found to be 3 at.% (*a* = 0.4087(1)-0.4101(1), *c* = 0.5159(2)-0.5173(2) nm) for 40 at.% Sn.

The phase relations in the V–Ni–Sn system at 773 K are characterized by the formation of the ternary stannide VNi_2Sn (see Fig. 3, Table 3), observed at the stoichiometric composition.

3.3. Electrical properties of the (V,Fe)Sn_2 compound

Electrical resistivity and thermopower (relative to pure copper) were measured for the $V_{0.55}Fe_{0.45}Sn_2$ phase in the temperature range 80-380 K. The temperature dependencies of the electrical resistivity and the thermopower are shown in Fig. 5. The compound shows metallic behavior in the investigated temperature range. The resistivity at room temperature is of the order of 1.80 μΩ m and with decreasing temperature it continuously decreases down to 80 K,

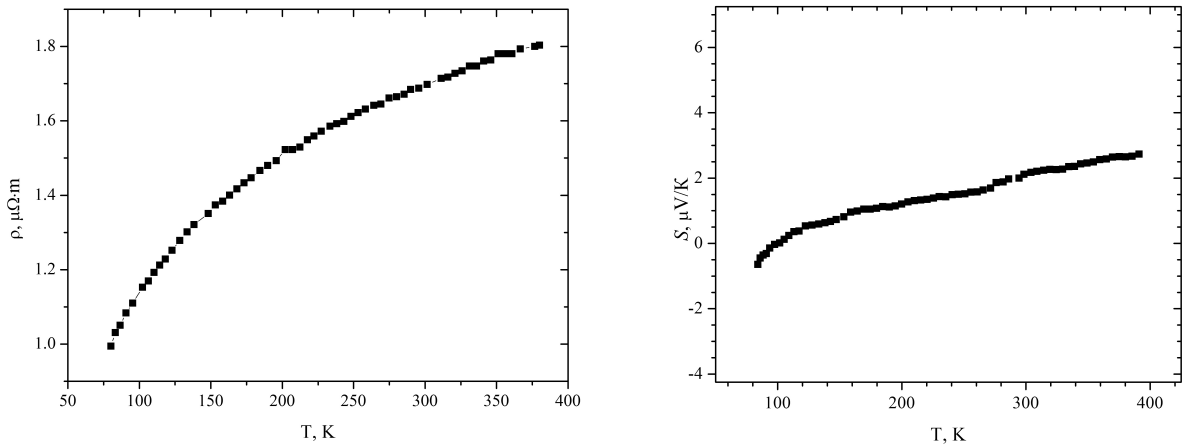

a b

Fig. 5 Temperature dependence of electrical resistivity (a) and thermopower (b) of $V_{0.55}Fe_{0.45}Sn_2$.

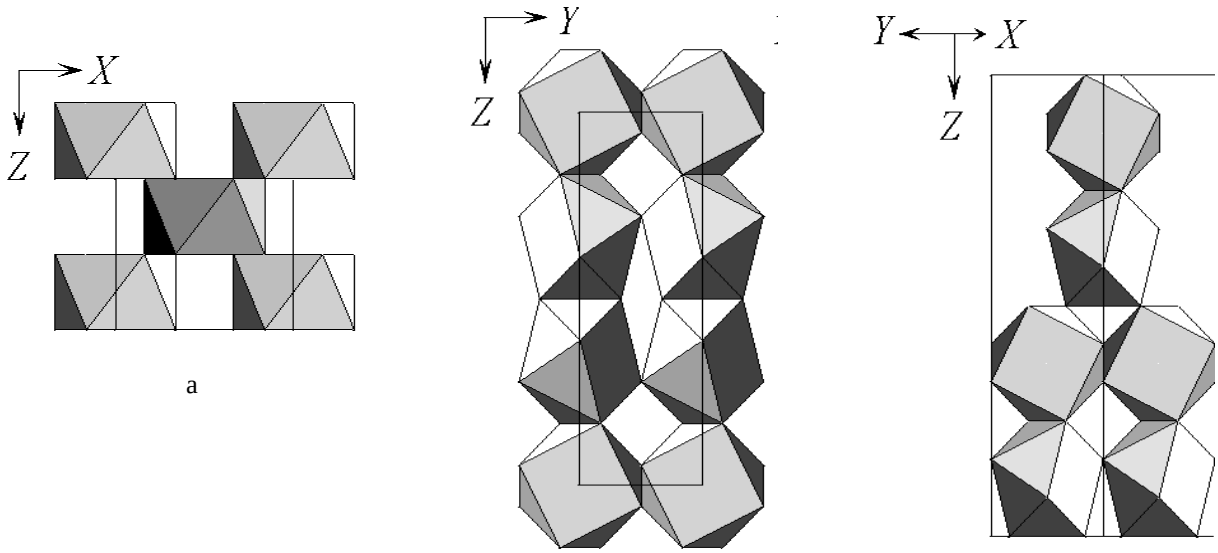

a b c

Fig. 6 Relationship between the structures of θ-$CuAl_2$, space group *I*4/*mcm* (a); Mg_2Ni, space group $P6_222$ (b); and Mg_2Cu, space group *Fddd* (c). Each tetragonal antiprism, formed by atoms of the majority element and centered by atoms of the minority element, is part of an infinite column of antiprisms sharing square faces.

where it reaches a value of about 0.994 μΩ m. The thermoelectric power of the studied compound is characterized by a small negative value (-0.64 μV/K) at 80 K. With increasing temperature it exhibits a continuous increase, becomes positive near 100 K and reaches a value of about 2.64 μV/K at 380 K, indicating the dominance of hole-type conductivity. The total change of the Seebeck coefficient is very small (~3 μV/K), which is consistent with the metallic character of the investigated stannide.

4. Final remarks

The $(V,Fe)Sn_2$ compound with Mg_2Ni-type was reported in [21], where a relatively broad region of existence, $V_{0.67(3)}Fe_{0.33(3)}Sn_2$ – $V_{0.52(3)}Fe_{0.48(3)}Sn_2$, was observed for samples prepared in tin flux. During our study of the V–Fe–Sn system the presence of the $(V,Fe)Sn_2$ compound with Mg_2Ni-type structure was confirmed at 873 K, where a slightly less broad homogeneity range was found. The authors of [21] studied several pseudo-binary stannide systems, $Ti_xV_{1-x}Sn_2$, $Ti_xFe_{1-x}Sn_2$, $V_xFe_{1-x}Sn_2$, $Cr_xMn_{1-x}Sn_2$, *etc.*, and analyzed the conditions of formation of the θ-$CuAl_2$-type, Mg_2Cu-type, Mg_2Ni-type, and $CoGe_2$-type, formed by the ternary and binary stannides. The influence of the valence electron concentration on the stability of the different structure types was emphasized. The former three structure types are characterized by tetragonal-antiprismatic coordination of the smaller atoms and can be described as packings

of columns of tetragonal antiprisms sharing the square faces. The relation between the structures of θ-$CuAl_2$, Mg_2Cu and Mg_2Ni is shown in Fig. 6. In the V–Fe–Sn system along the isoconcentrate of 67 at.% Sn, depending on the Fe/V content the three structures form: $FeSn_2$ (θ-$CuAl_2$-type), (V,Fe)Sn_2 (Mg_2Ni-type) and VSn_2 (Mg_2Cu-type) up to 786 K (peritectic melting point of $FeSn_2$). At 873 K we observed the ternary phase (V,Fe)Sn_2 (Mg_2Ni-type) and the binary phase VSn_2 with Mg_2Cu-type.

A comparison of the V–Fe–Sn and V–Ni–Sn systems studied here with other *Me*–*Me'*–Sn systems investigated earlier (*Me* = Ti, Zr, Hf; *Me'* = Fe, Co, Ni) shows that the Ti–Co–Sn and all the *Me*–Ni–Sn systems are characterized by the coexistence of two similar phases: *MeMe'*Sn with cubic MgAgAs-type structure (half-Heusler phases) and *MeMe'*$_2$Sn with cubic $MnCu_2Al$-type structure (Heusler phases). The *MeMe'*$_2$Sn Heusler phases are the thermodynamically dominating phases in the V–{Fe,Ni}–Sn, Ti–Fe–Sn and {Zr,Hf}–Co–Sn systems [23-27]. The formation of *MeMe'*Sn half-Heusler phases strongly depends on the electronic configuration of the d-metals, and the absence of V*Me'*Sn compounds in the V–{Fe,Ni}–Sn systems is probably due to this factor.

References

[1] J. Tobola, J. Pierre, *J. Alloys Compd.* 296 (2000) 243-252.

[2] K. Kaczmarska, J. Pierre, J. Tobola, *J. Magn. Magn. Mater.* 196-197 (1999) 627-628.

[3] V.V. Romaka, L. Romaka, Yu. Stadnyk, V. Gvozdetskii, R. Gladyshevskii, N. Skryabina, N. Melnychenko, V. Hlukhyy, T. Fässler, *Eur. J. Inorg. Chem.* (2012) 2588-2595.

[4] Yu. Stadnyk, A. Horyn, V. Sechovsky, L. Romaka, Ya. Mudryk, J. Tobola, T. Stopa, S. Kaprzyk, A. Kolomiets, *J. Alloys Compd.* 402 (2005) 30-35.

[5] K.H.J. Buschow, P.G. van Engen, R. Jongebreur, *J. Magn. Magn. Mater.* 38 (1983) 1-22.

[6] A.W. Carbonari, R.N. Saxena, W. Pendl Jr., J. Mestnik Filho, R.N. Attili, M. Olzon Dionysio, S.D. de Souza, *J. Magn. Magn. Mater.* 163 (1996) 313-321.

[7] P.G. van Engen, K.H.J. Buschow, M. Erman, *J. Magn. Magn. Mater.* 30 (1983) 374-382.

[8] *Pauling File*, MPDS, Switzerland, In: *Inorganic Solid Phases, SpringerMaterials* (on-line database), Springer, Heidelberg, 2014.

[9] F. Basile, P. Lecocq, A. Michel, *Ann. Chim. (Paris)* 4 (1969) 297-308.

[10] C. Wu, X. Su, J. Wang, Y. Liu, H. Tu, Y. Zhang, *J. Electron. Mater.* 43(11) (2014) 4111-4118.

[11] L. Akselrud, Yu. Grin. WinCSD: Software Package for Crystallographic Calculations (Version 4), *J. Appl. Crystallogr.* 47 (2014) 803-805.

[12] T.B. Massalski, H. Okamoto, P.R. Subramanian, L. Kacprzak (Eds.), *Binary Alloy Phase Diagrams*, ASM International, Metals Park, Ohio, 1990.

[13] P. Villars, L.D. Calvert (Eds.), *Pearson's Handbook of Crystallographic Data for Intermetallic Phases*, ASM International, Metals Park, Ohio, 1991.

[14] M. Singh, S. Bhan, *J. Mater. Sci. Lett.* 5 (1986) 733-735.

[15] K. Kanematsu, *Trans. Jpn. Inst. Met.* 27 (1986) 225-232.

[16] A.M. van der Kraan, D.B. de Mooij, K.H.J. Buschow, *Phys. Status Solidi A* 88 (1985) 231-237.

[17] B. Malaman, B. Roques, A. Courtois, J. Protas, *Acta Crystallogr. B* 32 (1976) 1348-1351.

[18] J. Maas, G. Bastin, F. van Loo, R. Metselaar, *Z. Metallkd.* 74 (1983) 294-299.

[19] R.M. Waterstrat, B. Dickens, *J. Appl. Phys.* 45 (1974) 3726-3728.

[20] S.K. Shadangi, M. Singh, S.C. Panda, S. Bhan, *Cryst. Res. Technol.* 21 (1986) 867-871.

[21] U. Häusssermann, S.I. Simak, I.A. Abrikosov, B. Johansson, S. Lidin, *J. Am. Chem. Soc.* 120 (1998) 10136-10146.

[22] M.K. Bhargava, K. Schubert, *J. Less-Common Met.* 33 (1973) 181-189.

[23] Yu.V. Stadnyk, L.P. Romaka, V.K. Pecharsky, R.V. Skolozdra, *Neorg. Mater.* 31 (1995) 1422-1425.

[24] L. Romaka, Yu.V. Stadnyk, O.I. Bodak, *J. Alloys Compd.* 317-318 (2001) 347-349.

[25] Yu.V. Stadnyk, R.V. Skolozdra, *Metally* (1) (1994) 164-167.

[26] Yu.V. Stadnyk, L.P. Romaka, *J. Alloys Compd.* 316 (2001) 169-171.

[27] L. Romaka, V.V. Romaka, Yu. Stadnyk, N. Melnychenko, *Chem. Met. Alloys* 6(1/2) (2013) 12-19.